JIPB Journal of Integrative Plant Biology

A leaf shape mutant provides insight into PINOID Serine/Threonine Kinase function in cucumber (*Cucumis sativus* L.)[FA]

Mengfei Song[†], Feng Cheng[†], Jing Wang, Qingzhen Wei, Wenyuan Fu, Xiaqing Yu, Ji Li, Jinfeng Chen* and Qunfeng Lou*

State Key Laboratory of Crop Genetics and Germplasm Enhancement, College of Horticulture, Nanjing Agricultural University, Nanjing 210095, China

[†]These authors contributed equally to the work.

*Correspondences: Jinfeng Chen (jfchen@njau.edu.cn); Qunfeng Lou (qflou@njau.edu.cn). Dr. Lou is fully responsible for the distribution of all materials associated with this article.

doi: 10.1111/jipb.12739

Abstract Optimizing leaf shape is a major challenge in efforts to develop an ideal plant type. Cucumber leaf shapes are diverse; however, the molecular regulatory mechanisms underlying leaf shape formation are unknown. In this study, we obtained a round leaf mutant (*rl*) from an ethyl methanesulfonate-induced mutagenesis population. Genetic analysis revealed that a single recessive gene, *rl*, is responsible for this mutation. A modified MutMap analysis combined linkage mapping identified a single nucleotide polymorphism within a candidate gene, *Csa1M537400*, as the mutation underlying the trait. *Csa1M537400* encodes a PINOID kinase protein involved in auxin transport. Expression of *Csa1M537400* was significantly lower in the *rl* mutant than in wild type, and it displayed higher levels of IAA (indole-3-acetic acid) in several tissues. Treatment of wild-type plants with an auxin transport inhibitor induced the formation of round leaves, similar to those in the *rl* mutant. Altered expression patterns of several auxin-related genes in the *rl* mutant suggest that *rl* plays a key role in auxin biosynthesis, transport, and response in cucumber. These findings provide insight into the molecular mechanism underlying the regulation of auxin signaling pathways in cucumber, and will be valuable in the development of an ideal plant type.

Edited by: Lars Ostergaard, John Innes Centre, UK
Received Sept. 21, 2018; **Accepted** Nov. 8, 2018; **Online on** Nov. 12, 2018
FA: Free Access

High-Impact Article

Free Access

INTRODUCTION

The leaf is the main plant organ for photosynthesis and one of the most important determinants of plant morphology. Leaf shape greatly affects plant architecture, photosynthetic area, fruit quality, and yield traits (Tsukaya 2006). Research into the molecular mechanisms underlying leaf shape regulation will provide important clues as to how to develop plants with ideal architecture. Numerous genes involved in leaf shape have recently been identified in *Arabidopsis*, maize (*Zea mays*), rice (*Oryza sativa*), tomato (*Solanum lycopersicum*), and pakchoi (*Brassica rapa*) (Ramirez et al. 2009; Zhang et al. 2009; Ben-Gera et al. 2012; Hui et al. 2012). The developmental status of leaf primordia, formed by the shoot apical meristems (SAM), largely determines final leaf morphology. *Class I KNOTTED-LIKE HOMEOBOX* genes (*KNOX1*), which are expressed both in the SAM and leaf primordia, regulate leaf shape (Uchida et al. 2010). In tomato, ectopic expression of *KNOX* genes, exclusively in the meristem and stem, resulted in a super-compound leaf (Hake et al. 2004).

Leaf shape diversity results largely from variation in leaf margins, and many genes have been proposed to influence the leaf margin. The occurrence of filamentous and furcated leaves and the loss of leaf margins in the *shoot organization2* (*sho2*) mutant suggested that *SHL4*/*SHO2* plays a crucial role in leaf domain development in rice (Itoh et al. 2008). *BrcCUC3*, a member of the *CUP-SHAPED COTYLEDON* (*CUC*) family, is involved in the

regulation of leaf margin and branch development in Chinese cabbage (Hui et al. 2012). Knock-out mutations in *MIR164A* result in leaves with deeper serrations when compared to the wild type in *Arabidopsis*. By contrast, gain-of-function *MIR164A* mutants develop leaves with smooth margins (Nikovics et al. 2006). Additional studies demonstrated that gain-of-function and knock-out mutants of other genes have the same phenotype as *mir164a*, including *DPA* (*DEVELOPMENT-RELATED PcG TARGET IN THE APEX*), *CUC2* (*CUP-SHAPED COTYLEDON2*), and *PIN1* (*PIN-FORMED1*) (Nikovics et al. 2006; Engelhorn et al. 2012).

The key phytohormone, auxin, has crucial roles in plant tropism, lateral organ development, apical dominance, differentiation of vascular tissue, embryo development, plant photomorphogenesis, and formation and maintenance of the root meristem (Balla et al. 2016). Several proteins are involved in auxin biosynthesis, transport, and response, such as AUXIN BINDING PROTEIN 1 (ABP1), AUXIN RESPONSE FACTOR (ARF), AUXIN TRANSPORTER PROTEIN 1 (AUX1), AUXIN TRANSPORTER-LIKE PROTEIN FAMILY (LAX) and PIN-FORMED PROTEINS (PIN) (Grones and Friml 2015). Several studies have shown that mutations in genes involved in auxin biosynthesis and transport can lead to phenotypic changes in leaf shape (Koenig et al. 2009; Jeong et al. 2012).

PIN proteins are thought to be auxin efflux transporters responsible for transporting auxin out of cells. PIN proteins also mediate auxin polar transport, which results in the formation of an auxin gradient along the plant axis (Gälweiler et al. 1998). PINOID (PID), a protein-serine/threonine kinase, is one of the known components of PIN in the plant polarity control mechanism (Zourelidou et al. 2014). PIDs are important regulators of plant architecture and reproduction in *Arabidopsis*, maize, and rice.

Earlier studies showed that PID mediates the process of phosphorylation, an essential intermediate step in the control of the polar targeting of PIN proteins (Michniewicz et al. 2007). Rice plants overexpressing *OsPID* exhibited an aberrant pattern of root development, curled and stunted shoots, a reduction in the number of stamens, and an increase in the number of stigmas. These results suggested that PID plays a role in pattern formation and organogenesis in the rice shoot (Morita and Kyozuka 2007).

In *Arabidopsis*, mutations in the *PIN1* and *PID* genes disrupted the bilateral symmetry and patterning of cotyledons (Furutani et al. 2004). Transgenic plants overexpressing *PID* showed elevated IAA content, which affected cell proliferation and expansion rates, resulting in reduced cell numbers and small-sized cells in the leaves. In contrast to the overexpression lines, knockout lines and *pid* mutants showed a slightly bigger rosette area, three cotyledons, and were sterile (Saini et al. 2017). *BARREN INFLORESCENCE2*, an ortholog of *PID*, is a key regulator of inflorescence and vegetative development in maize, and the *bif2* mutant has fewer branches, spikelets, florets, and floral organs (Mcsteen et al. 2007).

At present, cucumber are often densely cultivated and have a large degree of leaf stacking, which often affects photosynthesis, reducing photosynthetic yield, and ultimately affecting the economic benefits. Therefore, the ideal leaf shape is significant for cultivation patterns, rational close planting, and high photosynthetic efficiency of cucumber. The difference in leaf shape makes it easier for cucumber to adapt to different growth environments to achieve the best photosynthetic yield. Overexpression and RNA interference of the cucumber GATA3 family transcription factor gene *CsHAN1* (*HANABA TARANU*) resulted in leaf cracking (Ding et al. 2015). Small leaf size can adjust leaf temperature and moisture loss to resist heat stress in the cucumber *scl1* mutant, which lacks a protruded middle margin and displays small and cordate leaf.

The *SCL1* (*SMALL AND CORDATE LEAF 1*) gene was cloned by BSA (bulked segregant analysis)-seq technology, but its regulatory mechanism remains unclear (Gao et al. 2017). Using map-based cloning, Hou et al. (2017) identified *CsDET2* (*de-etiolated-2*) as the candidate gene affected in the cucumber dwarf mutant *scp-2* (*super compact-2*). CsDET2 is involved in the brassinosteroid (BR) regulatory pathway, and the loss-of-function mutant has wrinkled leaves. Likewise, the dwarf cucumber mutant *scp-1* displays round leaves with a wrinkled surface and unusual dark green color. *SCP-1* encodes a BR-C6-oxidase involved in BR biosynthesis (Wang et al. 2017).

In this study, we identified a round leaf mutant (*rl*) from an ethyl methanesulfonate (EMS)-mutagenized Changchunmici ('CCMC', North China type) cucumber population. In addition to round leaves, the mutant showed other visually distinctive phenotypes, including abnormal development of floral organs, fruit, and roots,

and female sterility. We demonstrate that the gene responsible for the *rl* locus encodes a PINOID kinase protein involved in auxin transport.

RESULTS

Phenotypic and genetic analysis of the *rl* mutant

A round leaf (*rl*) mutant was identified from an EMS mutant library. The *rl* mutant plants exhibit a distinctive, nearly-round leaf shape instead of the heart-shaped pentagon observed in wild-type (WT) plants (Figure 1). Some *rl* mutant plants have three cotyledons and a deformed first true leaf (Figure 1A). The mutant also exhibits abnormal development of floral organs, fruits, and roots (Figure 1B–D). Growth of the main root is weakened, and the number of lateral roots increased (Figure 1B). No sepal development is observed in male or female flowers of the *rl* mutant (Figure 1C, D). Cross sections of flowers revealed that the *rl* mutant is defective in sepal primordia differentiation from the apical meristem (arrows in Figure 2H–J) when compared to WT at the same growth stages. Homozygous *rl* mutants (*rlrl*) do not produce any seeds, but its pollen is fertile.

We next examined the phenotypes of F_1 and F_2 populations, generated from a cross between WT and *rl*, to identify the inheritance pattern of the *rl* phenotype. All F_1 progenies had WT phenotype, and 24 out of 78 plants of the F_2 population had a round-leaf phenotype. The wild-type versus round-leaf phenotypes segregated at a 3:1 ratio ($\chi^2 = 0.19$, $P = 0.66$), suggesting that the round-leaf trait is controlled by a single recessive gene.

Bulked segregant analysis-sequencing (BSA-seq) and MutMap analysis

For BSA-seq, a total of 10.4 Gb and 8.6 Gb of whole-genome sequencing data were generated from WT and *rl* pools, with genome coverages of 51.1- and 42.7-fold, respectively (Table S1). Short reads from the two DNA bulks were aligned to the '9930' reference genome to identify SNPs, and the Δ(SNP index) was calculated (Figure 3). To identify the causal region, the MutMap method was applied to analyze the SNP index graphs. The Δ (SNP indices) were randomly distributed, with

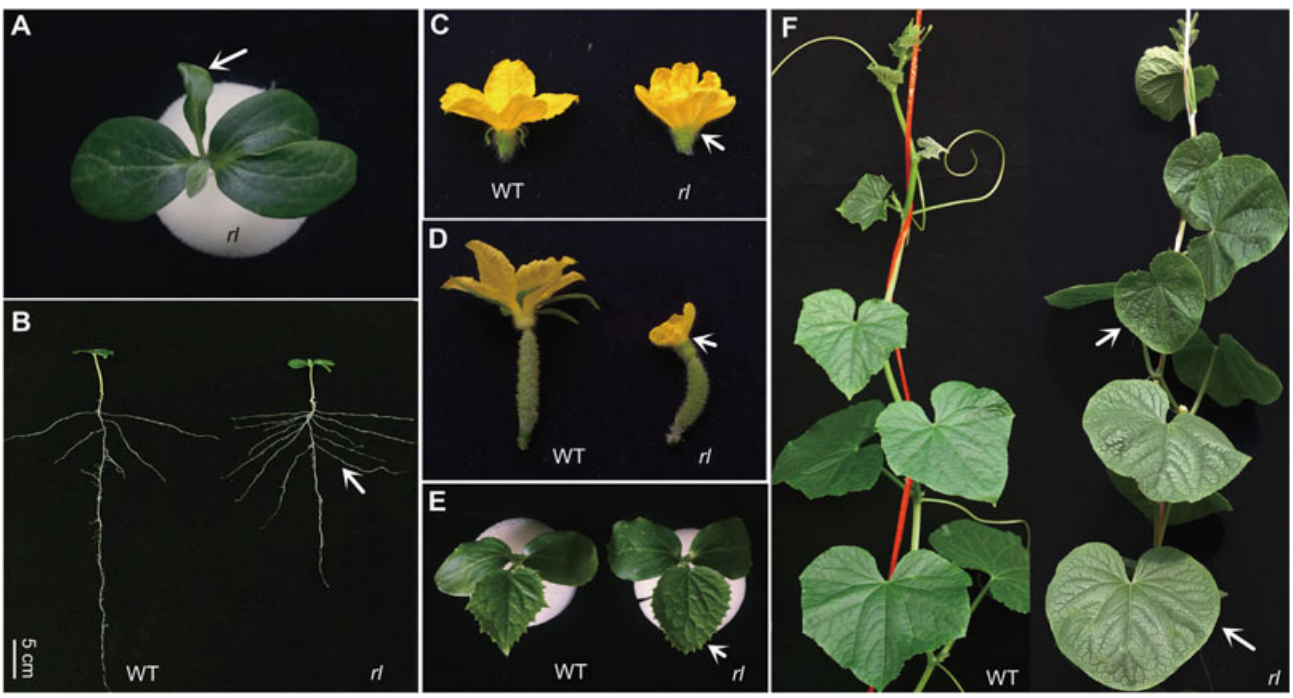

Figure 1. Phenotypic analysis of the *rl* mutant

Representative photographs of *rl* mutant cucumber plants showing abnormal development. **(A)** Cotyledons, **(B)** roots, **(C, D)** floral organs, **(D)** ovaries, and **(E)** first true leaf**. (F)** Plants at ten-leaf stage grown in the field. Arrows indicate the abnormal phenotypes in *rl* mutant.

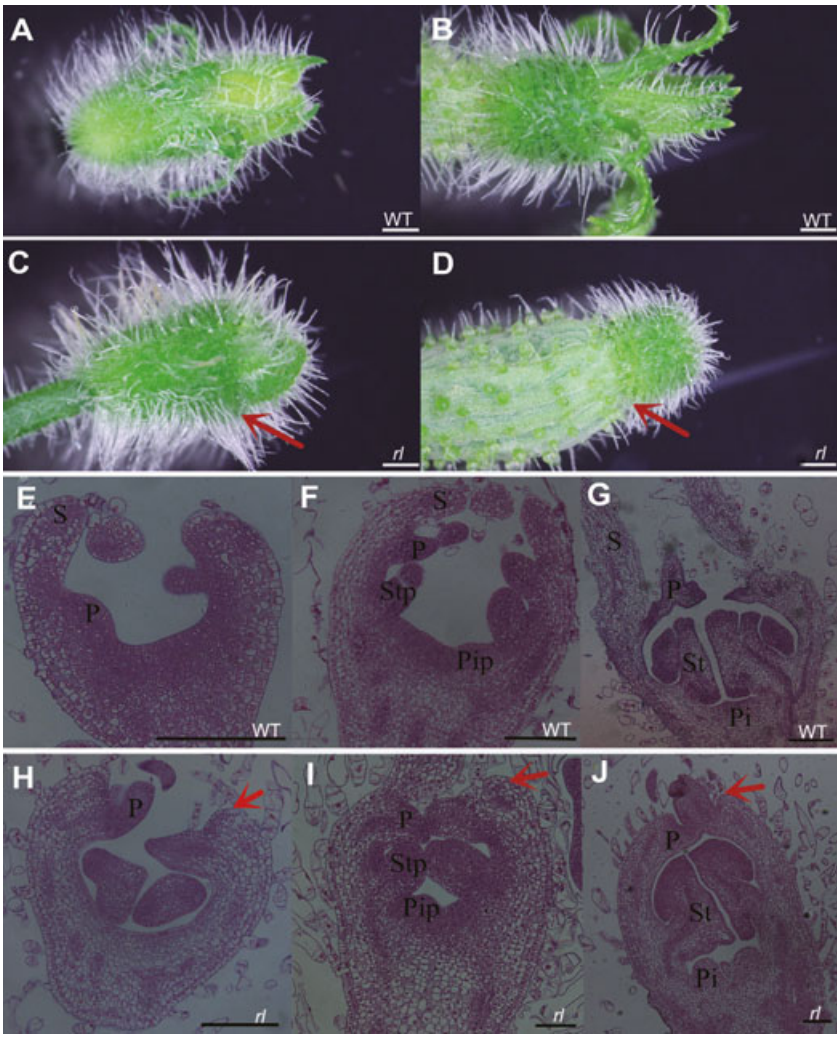

Figure 2. Abnormal flower phenotype of the *rl* mutant
Stereoscope images of **(A)** male and **(B)** female flowers of WT plants and **(C)** male and **(D)** female flowers of the *rl* mutant. Bar = 1 mm. **(E–J)** Micrographs of longitudinal sections of floral differentiation at the petal primordia differentiation stage **(E, H)**, the stamen and pistil primordia differentiation stage **(F, I)**, and the stamen and pistil developing stage **(G, J)**. Bar = 100 μm. S, sepal; P, petal; Stp, stamen primordia; Pip, pistil primordia; St, stamen; Pi, pistil. Arrows indicate defective sepal differentiation in the *rl* mutant.

low values (below 0.5) for most parts of the genome. A single genomic region harboring a cluster of SNPs with a high SNP index was identified in the 19.1–22.0 Mb interval of chromosome 1, suggesting that this candidate genomic region probably harbors the causative mutation.

Fine mapping of the *rl* gene

A new F_2 population containing 251 individuals (196 WT phenotype and 56 *rl* phenotype plants) was constructed from a cross between the *rl* mutant and 'hazerd' to narrow down the candidate region. Two polymorphic markers, UW083954 and SSR03680, were applied to identify 29 recombinants from these 251 F_2 individuals within the initial interval (Figure 4A). A total of 27 indel markers was developed within the initial interval, among which, 13 markers, showing obvious polymorphism between the two parents, were applied to genotype the 29 recombinants. Finally, fine mapping placed the *rl* locus in a genomic region flanked by markers rIndel5 and rIndel25, which was 165 kb in the '9930' cucumber reference genome (Figure 4B).

Based on the resequenced data of *rl* mutant pool, only two SNPs were detected in this region (Figure 4C).

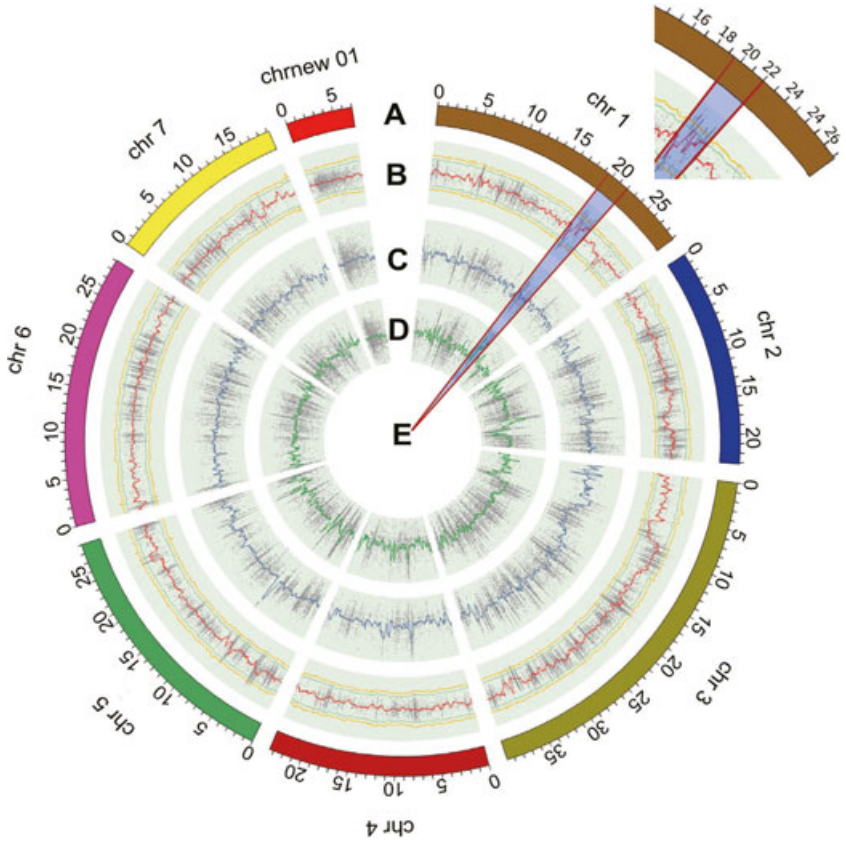

Figure 3. BSA-seq and MutMap analyses identified the *rl* locus

(A) Diagram of the seven cucumber chromosomes. **(B)** Δ (SNP index) plot with statistical confidence intervals under the null hypothesis of no SNP (Orange curve, $P \leq 0.01$; Green curve, $P \leq 0.05$). **(C)** SNP index of the WT pool. **(D)** SNP index of the *rl* pool. **(E)** Candidate interval (marked in blue). SNP indices were calculated based on a 1 Mb interval with a 10 kb sliding window, using the '9930' genome sequence as the reference genome.

Of these two SNPs, SNP (*SNP-1G19389144*) causes a non-synonymous homozygous mutation, and thus, was considered the causal SNP for the *rl* mutant. Another SNP (*SNP-1G19337224*), which was located in the intergenic region and had a low SNP index (0.6) in *rl* pool, was not further investigated.

Molecular cloning to identify SNP mutation

According to the Cucumber Genome Database, *SNP-1G19389144* is located on gene *Csa1M537400*. The gene structure consists of two exons and one intron (Figure 5A). To confirm the candidate mutation, the full-length cDNA of *Csa1M537400* was cloned from the *rl* mutant and WT. The *Csa1M537400* cDNA was 1,425 bp long in samples isolated from both the *rl* mutant and WT. Sequence alignments revealed one 'G' to 'A' base substitution, at position 1,092 bp in exon 2 of *Csa1M537400* (Figures 5, S1), resulting in an amino acid substitution from V (valine) to M (methionine), and corresponding to *SNP-1G19389144* (Figure 5B, C). Besides, the single nucleotide mutation of the candidate gene existed only in the *rl* mutant, but not in the other 74 natural populations (Figure S2). Amino acid sequence analysis indicated that *Csa1M537400* encodes a PINOID protein kinase containing a PKc-like superfamily domain at amino acid position 75–451. The amino acid mutation (position 345) occurred within this conserved domain, suggesting that it may affect protein function.

Tissue-specific expression of *Csa1M537400*

To investigate whether the mutation site (*SNP-1G19389144*) affects gene expression, we analyzed *Csa1M537400* expression in the stem, leaf, flower, root, and ovary of WT and *rl* plants using qRT-PCR analysis. In the WT, *Csa1M537400* expression was higher in the stem, leaf, and ovary, and lower in the root and

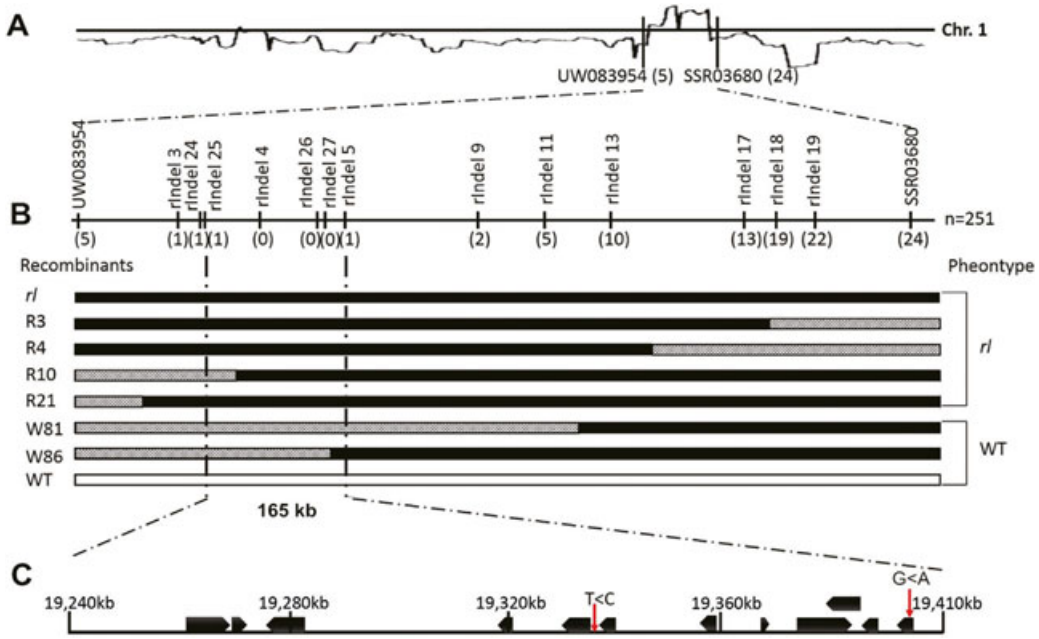

Figure 4. Genetic mapping of the *rl* gene

(A) Using two SSR markers, 29 recombinants were identified within the finial interval from 251 F_2 individuals. Black curve indicates the SNP index of the mutant pool. **(B)** The 29 recombinants and 15 polymorphic markers were applied to narrow down the *rl* locus to a 165 kb region. Values in parentheses indicates the number of recombinant plants of each marker. Black box indicates mutant genotype, white box the WT, and striped boxes for heterozygous genotype. **(C)** Physical position of the mapping region. Black arrows indicate genes, and red arrows indicate SNP mutations in the interval.

male flower (Figure 6). Compared to the WT, the expression levels of *Csa1M537400* were reduced significantly in all tissues of the *rl* mutant, especially in the leaf (11.8-fold decrease; Figure 6A).

To investigate the subcellular localization of the CsPID protein encoded by *Csa1M537400*, we expressed a PID-GFP fusion in onion epidermal cells. The PID-GFP fusion protein was localized in the membrane, cytoplasm, and nucleus of the onion cells, similar to the free GFP protein (Figure 6B).

Phylogenetic analysis of PINOID proteins from various plant species

To investigate its structural conservation and phylogenetic position, we used the predicted amino acid sequence of CsPID as a query to perform a BlastP search at NCBI. Twelve homologous protein sequences from other plant species, all of which contained a highest level of conserved PKc-like superfamily domain, were selected for further analysis (Figure S3). An alignment of these sequences revealed a high degree of conservation, varying from 92.91% (Melon homolog) to 60.12% (*Arabidopsis* homolog) relative to CsPID. A phylogenetic tree was constructed using the Neighbor-Joining (NJ) algorithm (Figure 7). The cucumber and melon PINOID proteins, which showed the highest percentage of identity in the alignment, clustered together.

PINOID kinase has been shown to regulate auxin transport at cellular membranes and its overexpression, or knockout, causes leaf growth defects in *Arabidopsis* (Saini et al. 2017). Similarly conserved domains and near evolutionary distance with high reliability indicate the PINOID proteins from other plants are orthologous, or paralogous, with that in cucumber and these proteins may have similar functions in regulating auxin transport and leaf growth.

Mutation of *Csa1M537400* alters IAA levels and expression profiles for genes associated with auxin synthesis, transport, and response

To examine whether *rl* is involved in the control of auxin transport, we determined the endogenous IAA content in different tissues of WT and *rl* mutant plants. The levels of IAA were highest in stems and lowest in

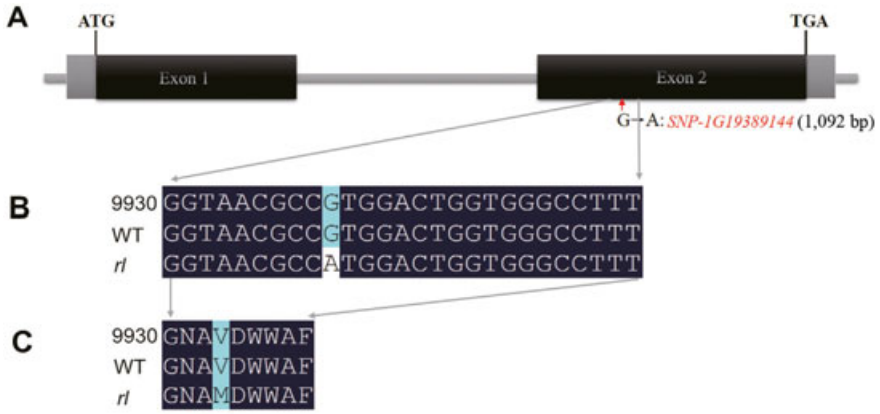

Figure 5. Single nucleotide polymorphism identified in *Csa1M537400* in the *rl* mutant

(A) Diagram of the *Csa1M537400* gene structure. Red arrow indicates the position of the single nucleotide mutation in the 2nd exon (*SNP-1G19389144*) of*Csa1M537400*. Gray boxes, black boxes, and lines between them indicate 5′ and 3′UTR, exons, and introns, respectively. **(B)** Sequence alignment of a fragment of the *RL* gene in the reference genome '9930', WT, and the *rl* mutant. **(C)** Alignment of predicted amino acid sequences from the gene fragment in **(B)** showing the V (valine) to M (methionine) substitution in the *rl* mutant.

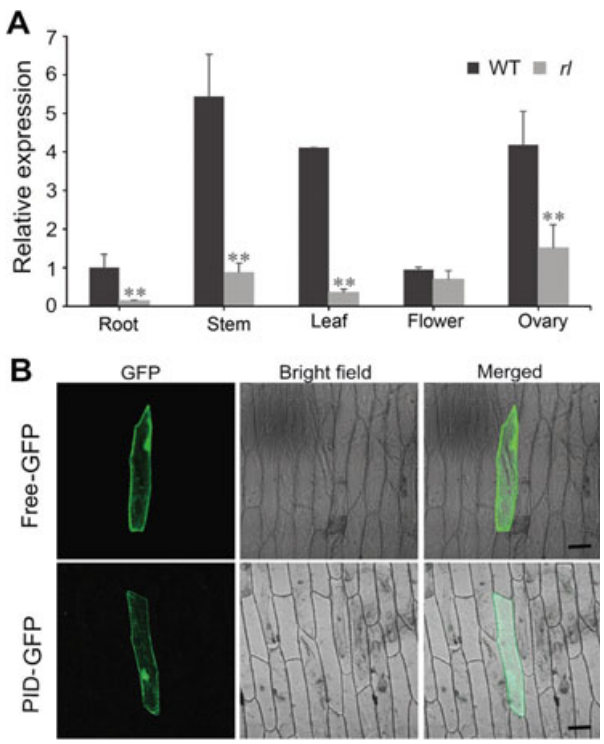

Figure 6. Expression pattern of *Csa1M537400*

(A) Relative expression of *Csa1M537400* in different tissues of WT and *rl* plants measured by qRT-PCR. Values are mean ± *SD* ($n = 3$ biological and 3 technical replicates). Asterisks indicate $P < 0.01$ (Student's *t*-test). **(B)** Subcellular localization of the PID protein encoded by *Csa1M537400*. A PID-GFP fusion protein was transiently expressed in onion epidermal cells, and GFP signal was observed by confocal fluorescence microscopy. Bar = 100 μm.

flowers in both WT and *rl* plants (Figure 8A). Compared with the WT, IAA levels in all tissues examined (root, stem, leaf, flower, and ovary) of the *rl* mutant were significantly higher (Figure 8A). This result suggests that the higher auxin levels are due to increased auxin biosynthesis, although other changes, such as altered transport or increased metabolism could also cause this observed change.

To identify which pathways of auxin synthesis and signaling are affected in the *rl* mutant, we examined the expression of 17 auxin-related genes in the leaves of 4-week-old WT and *rl* plants (Figure 8B). Three IAA synthesis-related genes, *YUCCA4* (pyridine nucleotide-disulphide oxidoreductase), *CYP79B3* (cytochrome P450 enzyme), and *NIT* (nitrilase); two auxin efflux genes, *PIN1* and *PIN2*; two auxin transporter-like genes, *AUX1a* and *AUX1b* (auxin influx carriers); two auxin transport inhibitor response genes, *TIR1a* and *TIR1b*; six auxin-induced primary transcripts genes, *AUX/IAA1*, *AUX/IAA2*, *SAUR1*, *SAUR2* (small auxin up RNA), *GH3a,* and *GH3b* (gretchen hagen3); and six auxin response factor genes, *ARF4*, *ARF6*, *ARF8*, *ARF10a*, *ARF10b*, and *ARF10c,* were selected.

Loss of function of CsPID resulted in significantly higher expression of three IAA synthesis genes, *YUCCA4*, *CYP79B3,* and *NIT*, and two auxin-induced primary transcript genes, *AUX/IAA1* and *SAUR2*. However, the expression levels of *PIN2*, *AUX1a*, *AUX1b,* and *ARF*s were lower in the *rl* mutant than in the WT. Expression levels of all six auxin-response factor genes were also

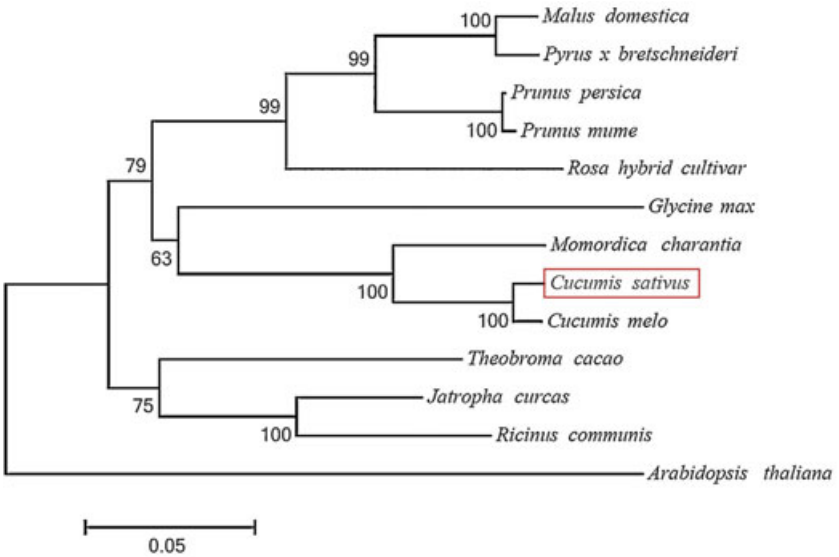

Figure 7. Phylogenetic relationships among PINOID proteins from different plant species
Phylogenetic tree inferred using the Neighbor-Joining method for 13 selected PINOID protein sequences. Numbers indicate the percentage of replicate trees in which the associated taxa clustered together in the bootstrap test (1,000 replicates). The tree is drawn to scale, and branch lengths indicate evolutionary distance. Evolutionary analyses were conducted in MEGA7.

significantly lower in the *rl* mutant. There was no significant difference between the WT and mutant in the expression of *PIN1*, *TIR1s*, *AUX/IAA2*, *SAUR*, and *GH3s*. These findings suggest that the *rl* mutation affects auxin biosynthesis, transport, and signaling.

Treatment with auxin transport inhibitors alters leaf shape in cucumber

To verify that the changes in leaf shape observed in the *rl* mutant are caused by the inactivation of auxin transport, WT plants were treated with five different concentrations of NPA, an auxin inhibitor (Figure 9). Wild-type 'CMCC' plants have heart-shaped pentagon leaves, with two pairs of symmetrical angles and a base angle. Under low concentrations of NPA, the first pair of symmetrical angles gradually flattened. Under higher concentrations of NPA, the second pair of symmetrical angles and the base angle also flattened, and the final leaf blade became nearly circular in shape.

DISCUSSION

Understanding the genetic mechanism of leaf shape is critical for modifying plant architecture and increasing crop yield. Studies have shown that genes related to leaf cell size and division, SAM differentiation, miRNA, and auxin polarity content influence leaf shape (Mao et al. 2014). Cucumber has a wide diversity of leaf shapes, and several studies have indicated that the molecular mechanisms underlying leaf shape in this plant involve SAM border control, nucleoside bisphosphate phosphatase, the BR regulatory pathway, miRNA, and auxin receptors (Ding et al. 2015; Gao et al. 2017; Hou et al. 2017; Xu et al. 2017).

In this study, a novel leaf shape mutant was identified from an EMS-induced mutagenesis population. When compared with the heart-pentagonal shape of WT leaves, the *rl* mutant exhibited round leaves and other organ defects (Figure 1F). Using genetic mapping and the MutMap method, we identified and cloned a single recessive gene controlling the *rl* mutation, *Csa1M537400*. A single nucleotide substitution (*SNP-1G19389144*) resulted in the lower transcript level in the mutation. Significant differences in *Csa1M537400* expression between WT and *rl* plants also supported this gene as the candidate gene of *rl* (Figure 6).

A modified MutMap method for the rapid identification of the *rl* mutation

A series of mapping methods, based on WGS (Whole-Genome Sequencing), have been reported, including

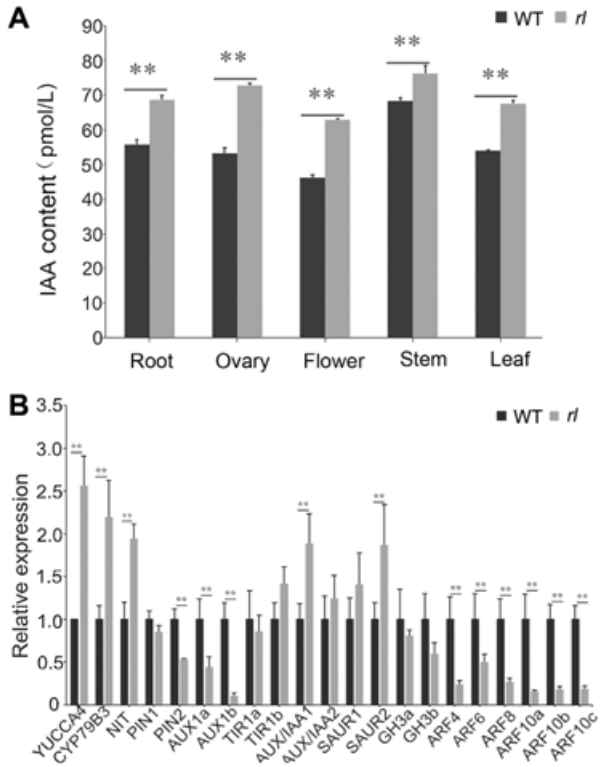

Figure 8. IAA content in *rl* and analysis of gene expression associated with auxin biosynthesis, transport, and response pathway

(A) Endogenous IAA content in different tissues of WT and *rl* mutant plants. Values are mean ± *SD*. $^{**}P < 0.01$ (Student's *t*-test). **(B)** Analysis by qRT-PCR of several auxin-related genes. Leaves of 4-week-old seedlings were sampled. Values are mean ± *SD* ($n = 3$ biological and 3 technical replicates). $^{**}P < 0.01$(Student's *t*-test).

SHOREmap (Schneeberger et al. 2009), NGM (Austin et al. 2011), MutMap (Abe et al. 2012), and MutMap-Gap (Takagi et al. 2013). MutMap can rapidly isolate the causal region by sequencing a DNA pool of mutant individuals from the F_2 progeny. However, it requires that the background material (WT) has a reference genome sequence.

In this study, we used a modified MutMap method, which only requires sequencing of mutant and wild-type pools. The sequenced reads were aligned to the '9930' reference genome sequence to calculate SNP indices, and then the two indices were subtracted to eliminate background interference (i.e., SNP mutations from 'CCMC' relative to the '9930' reference genome). The causal SNP (*SNP-1G19389144*) responsible for the mutant phenotype was rapidly identified within the interval identified using the modified MutMap method combined with linkage mapping (Figures 3, 4). This screening method, which focuses only on a candidate interval, is more time- and cost-efficient than other methods that rely on screening candidate SNPs in the whole genome.

The *rl* locus encodes a PINOID kinase protein

Functional and structural annotations showed that *Csa1M537400* encodes a serine/threonine protein kinase PINOID (PID) that contains a PKc-like superfamily domain that is highly conserved among homologous proteins from other species (Figure S2). Leaf development begins in cells in the area surrounding the SAM, and is regulated by levels of auxin (Reinhardt et al. 2000). As auxin efflux transporters, PINs are activated by D6 PROTEIN KINASE (D6PK) and PID kinases (Zourelidou et al. 2014). *PINOID* (*PID*) is a cloned protein-serine/threonine kinase gene belonging to the AGC kinase family in *Arabidopsis* (Michniewicz et al. 2007).

The main site of *PID* expression is the primordia of cotyledons, leaves, and flowers (Benjamins et al. 2001). Previous studies revealed that *PID* transcription is induced by exogenous auxin application (Benjamins et al. 2001; Friml et al. 2004). Furthermore, *pid* knockout mutants are deficient in PIN1 phosphorylation, and show pleiotropic growth defects related to leaves, cotyledons, embryo, roots, and flowers, and result in infertility in *Arabidopsis* (Benjamins et al. 2001; Friml et al. 2004; Lin et al. 2017). In this study, we demonstrate that a single amino acid substitution, within the PID functional domain, results in defects in multiple organs, suggesting that CsPID has a similar function to AtPID.

Auxin polar transport deficiency causes abnormal expression of several auxin-related genes, leading to changes in leaf shape

Several *pid* mutants exhibited defects in auxin transport (Morita and Kyozuka 2007). In this study, the content of IAA in different organs in the *rl* mutant differed from the WT, suggesting that *CsPID* is involved in the control of polar auxin transport in cucumber (Figure 8A). The molecular mechanisms of auxin-regulated leaf formation have been studied in many plant species. For instance, a mutation in the rice gene *NAL7*, a member of the *YUCCA* gene family known to regulate IAA biosynthesis, caused a significant decrease in the width

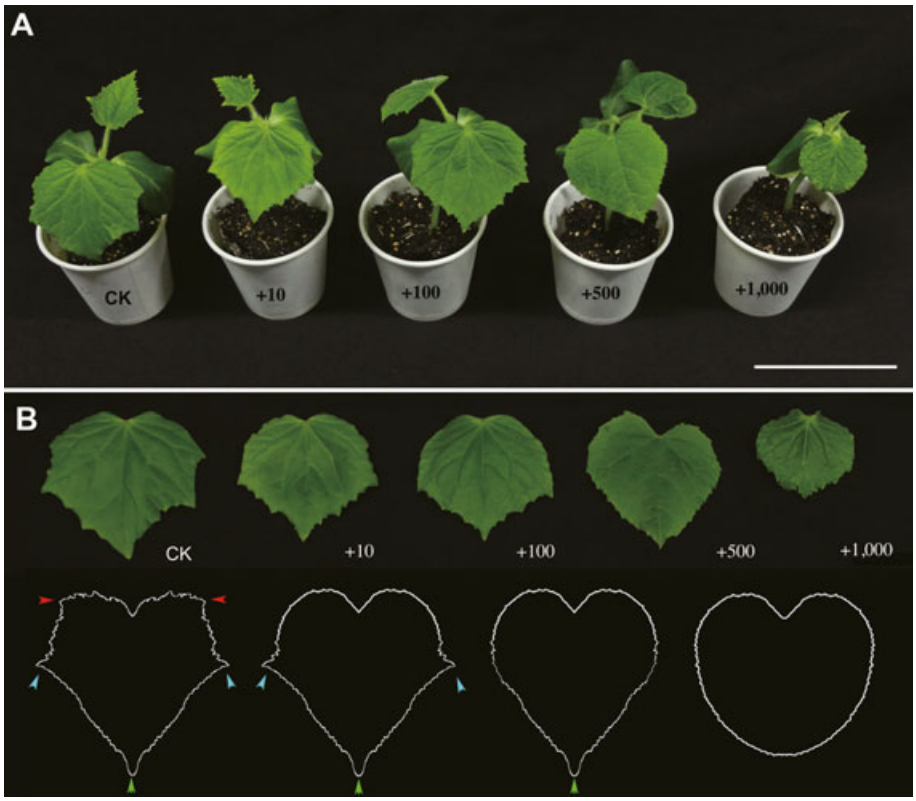

Figure 9. Effect of NPA treatment on leaf shape
(A) Morphology of WT plants at approximately 2 weeks after treatment with the indicated concentration of NPA. **(B)** Shape of cucumber leaves under different NPA concentrations. Red, blue, and green arrows refer to the three angles of the WT leaf, respectively. CK, control; +10, 100, 500, and 100 μmol/L: Scale bar = 5 cm.

of the leaf blade in rice (Fujino et al. 2008). *ENTIRE*, an inhibitory factor of the auxin response, regulates the morphological development of leaves by inhibiting the response to auxin between initiating leaflets in tomato (Koenig et al. 2009). The *Ln* gene, associated with the *Arabidopsis JAGGED* (*JAG*) homologous gene involved in auxin transport regulation, affects cell division and expansion, thereby regulating lateral organ development and leaf shape in maize (Jeong et al. 2012).

Loss of AUX1/LAX activity results in altered phyllotaxis, suggesting that auxin influx carriers (AUX1/LAX family) assist in maintaining regular phyllotaxis and organ initiation, at the shoot meristem (Bainbridge et al. 2008). PIN-mediated polar auxin transport is essential for the formation of blade angle (Bilsborough et al. 2011). Furthermore, CsPID is localized to all parts of the onion cell (Figure 6B), consistent with the pattern of auxin content. However, PID protein interacts with PIN protein on the plasma membrane in *Arabidopsis* (Wang et al. 2012).

The difference in the results of PID protein localization between onion and *Arabidopsis* may be caused by the application in heterologous plant cells. The best way is to use cucumber protoplasts for PID transient expression, but the cell wall of cucumber is very thick, so we could not prepare viable protoplasts. Thus, transient expression of PID in onion epidermal cells can only be used as reference. Treatment with auxin transport inhibitors altered the shape of wild-type leaves, from a heart-shaped pentagon into a circular shape (Figure 9). These observations suggest that the *rl* mutant is deficient in auxin polar transport.

A qRT-PCR analysis was conducted to probe whether the expression levels of auxin-related genes were affected in the *rl* mutant. Three genes showed significantly higher expression and 10 showed significantly lower expression in the *rl* mutant relative to WT (Figure 8B). Among them, expression of *YUCCA4* was 2.5-fold higher in the *rl* mutant relative to WT. YUCCCA proteins are rate-limiting enzymes in the main IAA

biosynthesis pathway in *Arabidopsis* (Mashiguchi et al. 2011). Over-expression of *YUUCCA* led to auxin-overproducing phenotypes, such as curled leaves and higher numbers of trichomes in Woodland Strawberry (Liu et al. 2014).

In this study, the higher expression of *YUCCA4* and two other IAA synthesis-related genes, *CYP79B3* and *NIT*, was consistent with the increase in IAA concentration, suggesting that *rl* is an auxin-overproducing mutant. Overexpression of *PID* would increase the IAA content in *Arabidopsis*, however, IAA content also increased in the *Arabidopsis pid* mutant (Saini et al. 2017). In cucumber, the expression levels of auxin synthesis-related genes was upregulated (Figure 8B). Therefore, IAA transport inhibition, caused by downregulation of the *PID* gene, is likely to increase IAA content by affecting auxin synthesis and related pathways, but the mechanism requires further study.

The early auxin-induced response genes, *SAUR*s, *GH3*-related transcript, and *Aux/IAA* are involved in signaling between auxin and downstream effectors (Woodward et al. 2005). *ARF*s can activate or inhibit the expression of other primary/early auxin response genes by interacting with auxin response elements (*AuxRE*) with these genes (Hagen and Guilfoyle 2002). In WT plants, as the concentration of auxin increases, auxin combines with *TIR* (auxin-transport inhibitor response), causing *Aux/IAA* ubiquitination and degradation, releasing the *ARF*s, and eventually promoting *ARF* gene expression (Wang et al. 2014; Saini et al. 2017). In the *rl* mutant, low expression of *ARF*s leads to a defect in a regulatory pathway that results in auxin overproduction.

CsPID affects development of flower structure

Except for the traditional ABCDE model genes, auxin-related genes also regulate floral organ formation. In *han*-2 mutant plants, reduced expression of the auxin response reporter and the unchanged expression of auxin transport revealed that *HAN* regulated flower development, via auxin response, but not through auxin transport (Zhang et al. 2013). Auxin related protein PIN-FORMED 1 (PIN1) and polar-localized protein PID adjusted auxin transport to control the boundary gene, *CUC1* and *CUC2*, in the formation of leaf and flower primordia. The expression of auxin response sensor and the dynamic distribution and localization of the auxin efflux transporter, PIN1, suggest that auxin plays a role in flower organ development and function (Goldentalcohen et al. 2017).

Mutation of *CsHAN* showed fused sepals and reduced floral organs in cucumber (Ding et al. 2015). In this study, high auxin levels and low expression of a target gene impeded calyx formation, but the down-regulation of gene expression is not significant, which may attribute to the fact that the gene is not abundantly expressed in floral organs. Further work should focus on how the *CsPID* gene interacts with the auxin pathway and floral development model genes to influence the development of flower structure.

In summary, we propose that a mutation in *CsPID* leads to a deficiency in auxin transport and, thereby, interferes with an auxin signaling pathway. The complex relationships between *rl* and other auxin-related genes deserves further investigation in the development of an ideal plant type.

MATERIALS AND METHODS

Plant materials and phenotypic data collection

The round leaf mutant (*rl*) was obtained from an M_2 generation of ethyl methanesulfonate (EMS)-treated plants of CCMC (changchunmici, North China type, WT). Since homozygous *rl* mutant plants are female infertile, WT (*RLRL* or *RLrl*) and mutant (*rlrl*) plants of the F_2 generation, from a cross between the *rl* mutant and WT plants, were used for phenotypic data collection and genetic analysis. A larger F_2 segregated population from the cross between the *rl* mutant and 'hazerd', a European greenhouse inbred line with heart-shaped pentagon leaf, were used to fine map of *rl* gene. All materials were grown in a greenhouse at Jiangpu Cucumber Research Station of Nanjing Agricultural University, Nanjing, China. Data were collected from individual plants. Subsequent data were analyzed using Microsoft Excel 2013.

BSA-sequencing and MutMap analysis

A modified MutMap method (Abe et al. 2012) was used to map *rl*. Genomic DNA was extracted from young leaves of F_2 individuals from the cross between *rl* and WT using the cetyltrimethyl ammonium bromide (CTAB) method (Murray and Thompson 1980). Equal amounts of DNA from 21 *rl* mutant individuals were bulked to generate the mutant pool and 24 WT individuals to

generate the wild-type pool for BSA-seq. Pair-end sequencing libraries with a read length of 100 bp and insert sizes of approx. 500 bp were subjected to whole-genome resequencing with Illumina HiSeq 2500. Short reads obtained from the two DNA pools were aligned against the cucumber genome sequence (the '9930' reference genome) to obtain the consensus sequence using BWA software (Huang et al. 2009). Reads from the *rl* and WT pools were separately aligned to the '9930' consensus sequence reads to call SNPs (Single Nucleotide Polymorphisms) using SAM tools software (Li et al. 2009). Aligned data were passed through a filter to reduce spurious SNP calls caused by sequencing and alignment errors based on the stringent selection criteria of read depth ≥ 7 and base sequencing quality scores ≥ 20.

SNP indices and Δ (SNP index) were calculated to determine the causal SNPs. The average SNP index and *P*-value in Chi-square tests for the SNPs in a certain genomic interval were calculated using a sliding window analysis with 1 Mb window size and 10 kb increment. Combined with the results of the SNP index curve and the Chi-square, the potential candidate region was identified.

Genetic mapping of *rl* candidate gene

A new F_2 population ($n = 251$) were applied to fine map *rl* locus from a cross between *rl* and 'hazerd', which was re-sequencing in our previous work. Based on the initial interval, two polymorphic SSR markers were developed at the two ends of the interval to screen recombinants (Cavagnaro et al. 2010). Indel markers were developed within the initial interval using resequenced data of parent 'hazerd'. Candidate SNPs were annotated using the Cucumber Genome Database (http://cucurbitgenomics.org/). All primers sequences are listed in Table S2.

Sequence analysis, annotation, and identification of the *rl* candidate gene

Total RNA was extracted from leaves of the *rl* mutant and WT plants using Trizol. cDNA was synthesized using a Prime Script TM RT Reagent Kit (TaKaRa) following the manufacturer's instructions. The coding sequences of the candidate genes from the *rl* mutant and WT were sequenced. DNA sequence of *Csa1G537400* among an additional 74 natural cucumber lines were obtained to verify the reliability of target mutant (Table S3). Full-length cDNA sequences and corresponding protein sequences were aligned, using the software DNAMAN. Functional annotations of candidate genes were acquired from the Cucumber Genome Database (http://cucurbitgenomics.org/) and NCBI (National Center for Biotechnology Information) databases (https://www.ncbi.nlm.nih.gov/). Functional domains of the protein were predicted by Pfam 31.0 online software (http://pfam.xfam.org/).

Measurement of endogenous IAA concentrations

Endogenous IAA concentrations were measured by Enzyme-linked immunosorbent assay (ELISA), as previously described (Maldiney et al. 1986). Endogenous IAA was measured from roots, stems, leaves, flowers, and ovaries of WT and *rl* mutant plants grown under the same conditions. One gram of tissue sample from each specimen was ground into a powder in liquid nitrogen and homogenized using 0.01 mol/L PBS (pH7.4), and then centrifuged for 20 min at 2,000–3,000 rpm. The supernatant was used to determine the IAA concentration; absorbance (O.D.) was measured in a spectrophotometer at a wavelength of 450 nm. The concentration of IAA in each sample was determined by comparing the O.D. value to a standard curve. Three technical replicates were conducted for each measurement.

Quantitative real-time PCR (qRT-PCR) analysis

Quantitative real-time PCR (qRT-PCR) was performed on tissue samples from the root, stem, leaf, male flower, and ovary from *rl* mutant and WT plants at the same growth stage. Quantitative real-time PCR was performed with a SYBR Premix Ex Taq^{TM} Kit (TaKaRa) in a Bio-Rad iQ1 Real-time PCR system (Bio-Rad) as described by Li et al. (2014), and the values from triplicate reactions were averaged. The threshold cycle (Ct) value of each gene was investigated and normalized to the Ct value of *Cs-Actin*. To determine relative expression fold differences for each gene during different treatments, the $2^{-\triangle\triangle}$Ct formula was applied. Relative mRNA expression data were analyzed using the Δ Ct method. Several auxin-related genes' primers were obtained based on Li et al. (2014). The primer sequences are listed in Table S2.

Subcellular localization of CsPID

To investigate the subcellular localization of CsPID in onion epidermal cells, the *CsPID* CDS was amplified from the pMD19-PID-T plasmid and fused with green fluorescent protein (GFP) to generate the plant binary

expression vector p35S::PID-GFP. The recombinant plant expression plasmid *p35S::PID-GFP* and a plasmid encoding free GFP, which was used as a negative control, were used for transient expression in onion epidermal cells via gene gun (Bio-Rad, PDS-1000/He, USA) bombardment. Bombarded onion epidermal cells were cultured on MS (Murashige and Skoog) medium and kept in darkness at 25°C for 14 h to allow transient expression of transgenes. Fluorescent signals were detected using a Zeiss LSM800 laser-scanning confocal microscope.

Phylogenetic analysis of *rl*

A phylogenetic tree was constructed using the amino acid sequences of predicted PINOID proteins from various plant species downloaded from the NCBI database (https://www.ncbi.nlm.nih.gov/). Multiple alignments of PINOID protein sequences were performed using DNAMAN software. A Neighbor-Joining tree was constructed with MEGA7.0.21 software using the neighbor-joining method based on 1,000 bootstrap replications (Saitou and Nei 1987).

Auxin transport inhibitor treatment

WT plants were exogenously sprayed with various concentrations (10, 100, 500, 1,000 μmol/L) of the auxin transport inhibitor, NPA (1-N-naphthylphthalamic acid, Sigma). For each treatment, plants were sprayed every 3 d after the cotyledons reached the fully expanded stage. Images and data on leaf shape were collected at the two-leaf stage.

Paraffin sections

Shoot tips of WT and *rl* mutant plants, grown under the same conditions, were sampled separately, fixed in 50% FAA fixation solution for at least 16 h and then embedded in paraffin, as previously described (Sun et al. 2010). The production process was repeated three times. Longitudinal sections of 3 μm thickness were mounted in neutral balsam. Haematoxylin Eosin (HE) staining results were examined and photographed using an OLYMPUS BX53 fluorescence microscope.

ACKNOWLEDGEMENTS

This research was partially supported by the National Natural Science Foundation of China (31430075, 31772318), the Fund for Independent Innovation of Agricultural Science and Technology of Jiangsu Province [CX(17)3016], and the National Supporting Programs (2016YFD0100204-25) from the Ministry of Science and Technology of China. The authors thank Martin Njogu (Department of Horticulture, College of Horticulture, Nanjing Agricultural University, Nanjing, China) for critical reading of the manuscript.

AUTHOR CONTRIBUTIONS

Q.L. and J.C. conceived the research and designed the experiments; M.S. and F.C. performed the research and analyzed the data; J.W. and W.F. performed the phenotypic selection, DNA extraction, and genetic mapping; Q.W., X.Q., and J.L. provided valuable experimental methods; all authors read and approved the final manuscript.

REFERENCES

Abe A, Kosugi S, Yoshida K, Natsume S, Takagi H, Kanzaki H, Matsumura H, Yoshida K, Mitsuoka C, Tamiru M, Innan H, Cano L, Kamoun S, Terauchi R (2012) Genome sequencing reveals agronomically important loci in rice using MutMap. **Nat Biotechnol** 30: 174–178

Austin RS, Vidaurre D, Stamatiou G, Breit R, Provart NJ, Bonetta D, Zhang J, Fung P, Gong Y, Wang PW, McCourt P, Guttman DS (2011) Next-generation mapping of *Arabidopsis* genes. **Plant J** 67: 715–725

Bainbridge K, Guyomarc'h S, Bayer E, Swarup R, Bennett M, Mandel T, Kuhlemeier C (2008) Auxin influx carriers stabilize phyllotactic patterning. **Genes Dev** 22: 810–823

Balla J, Medveďová Z, Kalousek P, Friml J, Reinöhl V, Procházka S (2016) Auxin flow-mediated competition between axillary buds to restore apical dominance. **Sci Rep** 6: 35955

Ben-Gera H, Shwartz I, Shao MR, Shani E, Estelle M, Ori N (2012) Entire and goblet promote leaflet development in tomato by modulating auxin response. **Plant J Cell Mol Biol** 70: 903–915

Benjamins R, Quint A, Weijers D, Hooykaas P, Offringa R (2001) The PINOID protein kinase regulates organ development in *Arabidopsis* by enhancing polar auxin transport. **Development** 128: 4057–4067

Bilsborough GD, Runions A, Barkoulas M, Jenkins HW, Hasson A, Galinha C, Laufs P, Hay A, Prusinkiewicz P, Tsiantis M (2011) Model for the regulation of *Arabidopsis thaliana* leaf margin development. **Proc Natl Acad Sci USA** 108: 3424–3429

Cavagnaro PF, Senalik DA, Yang L, Simon PW, Harkins TT, Kodira CD, Huang SW, Weng YQ (2010) Genome-wide

characterization of simple sequence repeats in cucumber (*Cucumis sativus* L.). **BMC Genomics** 11: 569

Ding L, Yan S, Jiang L, Liu M, Zhang J, Zhao J, Zhao W, Han Y, Wang Q, Zhang X (2015) *HANABA TARANU* regulates the shoot apical meristem and leaf development in cucumber (*Cucumis sativus* L.). **J Exp Bot** 66: 7075–7087

Engelhorn J, Reimer JJ, Leuz I, Göbel U, Huettel B, Farrona S, Turck F (2012) *DEVELOPMENT-RELATED PcG TARGET IN THE APEX 4* controls leaf margin architecture in *Arabidopsis thaliana*. **Development** 139: 2566–2575

Friml J, Yang X, Michniewicz M, Weijers D, Quint A, Tietz O, Benjamins R, Ouwerkerk PB, Ljung K, Sandberg G, Hooykaas PJ, Palme K, Offringa R (2004) A PINOID-dependent binary switch in apical-basal PIN polar targeting directs auxin efflux. **Science** 306: 862–865

Fujino K, Matsuda Y, Ozawa K, Nishimura T, Koshiba T, Fraaije MW, Sekiguchi H (2008) *NARROW LEAF 7* controls leaf shape mediated by auxin in rice. **Mol Genet Genomics** 279: 499–507

Furutani M, Vernoux T, Traas J, Kato T, Tasaka M, Aida M (2004) PIN-FORMED1 and PINOID regulate boundary formation and cotyledon development in *Arabidopsis* embryogenesis. **Development** 131: 5021

Gälweiler L, Guan C, Müller A, Wisman E, Mendgen K, Yephremov A, Palme K (1998) Regulation of polar auxin transport by AtPIN1 in *Arabidopsis* vascular tissue. **Science** 282: 2226–2230

Gao D, Zhang C, Zhang S, Hu B, Wang S, Zhang Z, Huang S (2017) Mutation in a novel gene *SMALL AND CORDATE LEAF 1* affects leaf morphology in cucumber. **J Integr Plant Biol** 59: 736–741

Goldentalcohen S, Israeli A, Ori N, Yasuor H (2017) Auxin response dynamics during wild-type and entire flower development in tomato. **Plant Cell Physiol** 58: 1661

Grones P, Friml J (2015) Auxin transporters and binding proteins at a glance. **J Cell Sci** 128: 1–7

Hagen G, Guilfoyle T (2002) Auxin-responsive gene expression: Genes, promoters and regulatory factors. **Plant Mol Biol** 49: 373–385

Hake S, Smith HM, Holtan H, Magnani E, Mele G, Ramirez J (2004) The role of knox genes in plant development. **Annu Rev Cell Dev Biol** 20: 125–151

Hou S, Niu H, Tao Q, Wang S, Gong Z, Li S, Weng Y, Li Z (2017) A mutant in the *CsDET2* gene leads to a systemic brassinosteriod deficiency and super compact phenotype in cucumber (*Cucumis sativus* L.). **Theor Appl Genet** 130: 1693–1703

Huang S, Li R, Zhang Z, Li L, Gu X, Fan W, Lucas WJ, Wang X, Xie B, Ni P, Ren Y, Zhu H, Li J, Lin K, Jin W, Fei Z, Li G, Staub J, Kilian A, van der Vossen EA, Wu Y, Guo J, He J, Jia Z, Ren Y, Tian G, Lu Y, Ruan J, Qian W, Wang M, Huang Q, Li B, Xuan Z, Cao J, Asan, Wu Z, Zhang J, Cai Q, Bai Y, Zhao B, Han Y, Li Y, Li X, Wang S, Shi Q, Liu S, Cho WK, Kim JY, Xu Y, Heller-Uszynska K, Miao H, Cheng Z, Zhang S, Wu J, Yang Y, Kang H, Li M, Liang H, Ren X, Shi Z, Wen M, Jian M, Yang H, Zhang G, Yang Z, Chen R, Liu S, Li J, Ma L, Liu H, Zhou Y, Zhao J, Fang X, Li G, Fang L, Li Y, Liu D, Zheng H, Zhang Y, Qin N, Li Z, Yang G, Yang S, Bolund L, Kristiansen K, Zheng H, Li S, Zhang X, Yang H, Wang J, Sun R, Zhang B, Jiang S, Wang J, Du Y, Li S (2009) The genome of the cucumber, *Cucumis sativus* L. **Nat Genet** 41: 1275–U1229

Hui MX, Zhang LG, Yu X, Wang H, Bai JJ, He YK (2012) Cloning of *BrcCUC3* from *Brassica rapa* ssp. chinensis and its effect on leaf morphology and inflorescence structure. **J Agric Biotechnol** 20: 337–346

Itoh JI, Sato Y, Nagato Y (2008) The *SHOOT ORGANIZATION2* gene coordinates leaf domain development along the central-marginal axis in rice. **Plant Cell Physiol** 49: 1226–1236

Jeong N, Suh SJ, Kim MH, Lee S, Moon JK, Kim HS, Jeong SC (2012) Ln is a key regulator of leaflet shape and number of seeds per pod in soybean. **Plant Cell** 24: 4807–4818

Koenig D, Bayer E, Kang J, Kuhlemeier C, Sinha N (2009) Auxin patterns Solanum lycopersicum leaf morphogenesis. **Development** 136: 2997–3006

Li H, Durbin R (2009) Fast and accurate short read alignment with Burrows-Wheeler transform. **Bioinformatics** 25: 1754–1760

Li J, Wu Z, Cui L, Zhang T, Guo Q, Xu J, Jia L, Lou Q, Huang S, Li Z, Chen J (2014) Transcriptome comparison of global distinctive features between pollination and parthenocarpic fruit set reveals transcriptional phytohormone cross-talk in cucumber (*Cucumis sativus* L.). **Plant Cell Physiol** 55: 1325–1342

Lin F, Xu D, Jiang Y, Chen H, Fan L, Holm M, Deng XW (2017) Phosphorylation and negative regulation of CONSTITUTIVELY PHOTOMORPHOGENIC 1 by PINOID in *Arabidopsis*. **Proc Natl Acad Sci USA** 114: 6617–6622

Liu H, Xie WF, Zhang L, Valpuesta V, Ye ZW, Gao QH, Duan K (2014) Auxin biosynthesis by the *YUCCA6* flavin monooxygenase gene in woodland strawberry. **J Integr Plant Biol** 56: 350–363

Maldiney R, Leroux B, Sabbagh I, Sotta B, Sossountzov L, Miginiac E(1986) A biotin-avidin-based enzyme immunoassay to quantify three phytohormones: Auxin, abscisic acid and zeatin-riboside. **J Immunol Methods** 90: 151–158

Mao Y, Wu F, Yu X, Bai J, Zhong W, He Y (2014) MicroRNA319a-targeted *Brassica rapa* ssp pekinensis *TCP* genes modulate head shape in Chinese cabbage by differential cell division arrest in leaf regions. **Plant Physiol** 164: 710–720

Mashiguchi K, Tanaka K, Sakai T, Sugawara S, Kawaide H, Natsume M, Hanadaa A, Yaenoa T, Shirasua K, Yaod H, McSteend P, Zhaoe Y, Hayashif K, Kamiyaa Y, Kasaharaa H (2011) The main auxin biosynthesis pathway in *Arabidopsis*. **Proc Natl Acad Sci USA** 108: 18512–18517

Mcsteen P, Malcomber S, Skirpan A, Lunde C, Wu X, Kellogg E, Hake S (2007) *barren inflorescence2* encodes a co-ortholog of the *PINOID* serine/threonine kinase and is required for organogenesis during inflorescence and vegetative development in maize. **Plant Physiol** 144: 1000–1011

Michniewicz M, Zago MK, Abas L, Weijers D, Schweighofer A, Meskiene, I, Heisler MG, Ohno C, Zhang J, Huang F, Schwab R, Weigel D, Meyerowitz EM, Luschnig C, Offringa R, Friml J (2007) Antagonistic regulation of PIN

phosphorylation by PP2A and PINOID directs auxin flux. **Cell** 130: 1044–1056

Morita Y, Kyozuka J (2007) Characterization of OsPID, the rice ortholog of PINOID, and its possible involvement in the control of polar auxin transport. **Plant Cell Physiol** 48: 540–549

Murray MG, Thompson WF (1980) Rapid isolation of high molecular weight plant DNA. **Nucleic Acids Res** 8: 4321–4325

Nikovics K, Blein T, Peaucelle A, Ishida T, Morin H, Aida M, Laufs P (2006) The balance between the *MIR164A* and *CUC2* genes controls leaf margin serration in *Arabidopsis*. **Plant Cell** 18: 2929–2945

Ramirez J, Bolduc N, Lisch D, Hake S (2009) Distal expression of knotted1 in maize leaves leads to reestablishment of proximal/distal patterning and leaf dissection. **Plant Physiol** 151: 1878–1888

Reinhardt D, Mandel T, Kuhlemeier C (2000) Auxin regulates the initiation and radial position of plant lateral organs. **Plant Cell** 12: 507–518

Saini K, Markakis MN, Zdanio M, Balcerowicz DM, Beeckman T, De Veylder L, Prinsen E, Beemster GTS, Vissenberg K (2017) Alteration in auxin homeostasis and signaling by overexpression of PINOID kinase causes leaf growth defects in *Arabidopsis thaliana*. **Front Plant Sci** 8: 1009

Saitou N, Nei M (1987) The neighbor-joining method: A new method for reconstructing phylogenetic trees. **Mol Biol Evol** 4: 406–425

Schneeberger K, Ossowski S, Lanz C, Juul T, Petersen AH, Nielsen KL, Jorgensen JE, Weigel D, Andersen SU (2009) SHOREmap: Simultaneous mapping and mutation identification by deep sequencing. **Nat Methods** 6: 550–551

Sun CQ, Chen FD, Teng NJ, Liu ZL, Fang WM, Hou XL (2010) Factors affecting seed set in the crosses between *Dendranthema grandiflorum* (Ramat.) Kitamura and its wild species. **Euphytica** 171: 181–192

Takagi H, Uemura A, Yaegashi H, Tamiru M, Abe A, Mitsuoka C, Utsushi H, Natsume S, Kanzaki H, Matsumura H, Saitoh H, Yoshida K, Cano LM, Kamoun S, Terauchi R (2013) MutMap-Gap: Whole-genome resequencing of mutant F_2 progeny bulk combined with de novo assembly of gap regions identifies the rice blast resistance gene Pii. **New Phytol** 200: 276–283

Tsukaya H (2006) Mechanism of leaf-shape determination. **Ann Rev Plant Biol** 57: 477–496

Uchida N, Kimura S, Koenig D, Sinha N (2010) Coordination of leaf development via regulation of *KNOX1* genes. **J Plant Res** 123: 7

Wang B, Henrichs S, Geisler M (2012) The AGC kinase, PINOID, blocks interactive ABCB/PIN auxin transport. **Plant Signal Behav** 7: 1515–1517

Wang H, Li WQ, Qin YG, Pan Yp, Wang XF, Weng YQ, Chen P, Li Y (2017) The cytochrome P450 gene *CsCYP85A1* is a putative candidate for super compact-1 (*scp-1*) plant architecture mutation in cucumber (*Cucumis sativus* L.). **Front Plant Sci** 8: 266

Wang RH, Estelle M (2014) Diversity and specificity: Auxin perception and signaling through the TIR1/AFB pathway. **Curr Opin Plant Biol** 21: 51–58

Woodward AW, Bartel B (2005) Auxin: Regulation, action, and interaction. **Ann Bot** 95: 707–735

Xu J, Li J, Li C, Zhang T, Wu Z, Zhu PY, Meng YJ, Zhang KJ, Yu XQ, Lou QF, Chen JF (2017) New insights into the roles of cucumber TIR1 homologs and *miR393* in regulating fruit/seed set development and leaf morphogenesis. **BMC Plant Biol** 17: 130

Zhang GH, Xu Q, Zhu XD, Qian Q, Xue HW (2009) SHALLOT-LIKE1 is a KANADI transcription factor that modulates rice leaf rolling by regulating leaf abaxial cell development. **Plant Cell** 21: 719–735

Zhang XL, Zhou Y, Ding L, Wu ZG, Liu RY, Meyerowitz EM (2013) Transcription repressor HANABA TARANU controls flower development by integrating the actions of multiple hormones, floral organ specification genes, and GATA3 family genes in *Arabidopsis*. **Plant Cell** 25: 83–101

Zourelidou M, Absmanner B, Weller B, Barbosa IC, Willige BC, Fastner A, Streit V, Port SA, Colcombet J, Bentem SF, Hirt H, Kuster B, Schulze WX, Hammes UZ, Schwechheimer C (2014) Auxin efflux by PIN-FORMED proteins is activated by two different protein kinases, D6 PROTEIN KINASE and PINOID. **Elife** 19: 3

SUPPORTING INFORMATION

Additional Supporting Information may be found online in the supporting information tab for this article: http://onlinelibrary.wiley.com/doi/10.1111/jipb.12739/suppinfo

Figure S1. Alignment of cDNA sequences for *Csa1M537400* isolated from three cucumber genotypes: 9930, WT and the *rl* mutant

Figure S2. Partial DNA sequence alignment of *Csa1M537400* among 74 lines of the natural cucumber population, 9930, ccmc and *rl*. The SNP mutant sites are marked with red boxes

Figure S3. Predicted amino acid sequence alignment of 13 PINOID proteins. The PKc-like Superfamily domain is enclosed in a red box

Table S1. Whole genome sequencing reports for the *rl* and WT pools

Table S2. Primer sequences used in this study

Table S3. Information of 74 non-round leaf *Cucumis* species from a natural population